

Density contrast and jet morphology in 3C 273

S. Jester

Fermilab, MS 127, PO Box 500, Batavia IL, 60510, USA

`jester@fnal.gov`

and

M. Krause

Landessternwarte Königstuhl, 69117 Heidelberg, Germany

`M.Krause@lsw.uni-heidelberg.de`

ABSTRACT

We present an axisymmetric 2.5D hydrodynamical simulation of a twin jet propagating in a King atmosphere. The jet is initially underdense but becomes overdense in the decreasing external density profile. A shock forms near this crossover position, compressing the jet plasma. Simultaneously, filaments of jet material are disconnected from the main flow by nonlinear Kelvin-Helmholtz instabilities at the interface between the jet's cocoon and the shocked ambient medium. These mechanisms explain the morphology of 3C 273's kiloparsec-scale jet, in which bright radio, optical and X-ray emission sets on halfway along the jet. We suggest that the shock identified in the simulation is the cause of the sudden onset of bright emission, and possibly the energy source for the jet's brightest X-rays. We further identify the jet's elusive extensions with the filaments in the simulation. Within our model, it is possible to determine key physical parameters directly which are otherwise difficult to access, in particular the jet density and bulk Lorentz factor. We outline future observations to confirm our model, and thus our determination of physical parameters for a relativistic jet.

Subject headings: Hydrodynamics – Instabilities – Shock waves – Galaxies: jets
– Quasars: individual: 3C 273

1. Introduction

In the standard model for Active Galactic Nuclei, jets transfer mass, energy (kinetic and electromagnetic) and momentum from the central object into the surrounding medium. Several hundreds of jets have been detected so far, nearly exclusively by their radio synchrotron emission (Liu & Zhang 2002). VLBI observations of apparent superluminal motion show that the jets must be relativistic at least at these small scales (Zensus 1997). A subclass of about 25 jets shows optical synchrotron emission (Jester 2003)¹. X-ray emission has been detected from a similar number, including some of the optical jets. Here, the emission mechanism is either assumed to be synchrotron emission, too, or explained as inverse Compton scattering of microwave background photons, which requires the relativistic motion to persist out to kiloparsec scales (Harris & Krawczynski 2002). While high-resolution data are now available at radio, optical and X-ray wavelengths, the detailed physical parameters of the jet flow are not simple observables. Similarly, there is no generally accepted model explaining the morphology of jets, which usually appear to consist of bright knots linked by more diffuse emission, although specific models have been brought forward for specific sources (*e.g.*, Königl & Choudhuri 1985; Lobanov & Zensus 2001).

One of the best studied jets is that associated with the quasar 3C 273 (Fig. 1; Jester et al. 2001, 2002, and references therein). A single radio jet extends continuously over $21''4$ from core to hot spot, while easily detectable optical and X-ray emission are only observed at $r \gtrsim 12''$ from the core, setting on fairly abruptly at a feature called “knot A” (Fig. 1). Beyond knot A, the optical jet appears helical, with constant outer radius. The optical brightness is approximately constant. Knot A is the location of the brightest X-ray emission peak, with a further peak at B1, and nearly constant brightness at larger radii. As a further remarkable feature of knot A, an optical “extension” *S* appears to emanate from it to the south. There is further an “inner extension” *In*, consisting of two knots, to the north. No X-ray or radio emission comparable to the jet’s has been detected from these extensions. The infrared-optical spectral energy distributions of *S* and *In*’s southern knot *In1* are so hard that the presence of radio emission from them cannot be excluded on the basis of presently available radio maps (Jester et al. 2001).

Although the jet in 3C 273 meets the Fanaroff & Riley (1974) type II criteria, it does not have a prominent radio lobe. There is, however, a faint but highly polarised steep-spectrum emission component, tentatively identified as a backflow (Röser, Conway, & Meisenheimer 1996). This backflow also accounts for the different width of 3C 273’s jet at radio and optical wavelengths: at $0''.3$ resolution, the optical jet has a cross-sectional full-width at half

¹Also see <http://home.fnal.gov/~jester/optjets/> for a current list of optical jets.

maximum brightness of $0''.5$, while the radio jet is approximately $0''.2$ wider. The backflow develops into the diffuse radio emission to the south of knot A (Figure 1).

In non-relativistic simulations, jets lighter than the surrounding medium (density contrast $\eta < 1$) are known to produce considerable backflows. In contrast, their heavy (overdense, $\eta > 1$) relatives only have a small backflow, tightly wrapped around the jet beam (Norman, Winkler, & Smarr 1983). While it is possible to suppress the production of radio lobes by magnetic fields with the appropriate toroidal field configuration (Clarke 1993), this has not been shown to work with very underdense jets (Tregillis, Jones, & Ryu 2001). Thus, with its lack of a lobe and the presence of only a weak backflow, 3C 273’s kiloparsec-scale jet has a morphology typical for a heavy jet.

3C 273’s host galaxy is part of a poor group including four other members (Stockton 1980). Fitting a King profile to ROSAT data, Röser et al. (2000) deduced that 3C 273 resides in an X-ray atmosphere with a central particle density of $6 \times 10^4 \text{ m}^{-3}$ and a scale length of approximately $10''$. This means that knot A is located in a region of decreasing external density. Like other radio jets, this jet is originally underdense as it moves through the innermost regions of the quasar’s host galaxy. As noted above, the jet’s radio morphology shows that it is overdense at its largest distance from the quasar core.

We have developed a model in which the prominent knot A appears at the point where the external density has dropped off to equal that in the jet, so that the originally underdense jet is indeed overdense at larger distances from the core. The disturbance in the backflow near the transition region will then lead to a shock in the jet, lighting up the jet near region A. Such an underdense-overdense transition would be predicted from the central density given by Röser et al. (2000) and the line-of-sight angle of $\approx 3^\circ$ determined by Harris & Krawczynski (2002) from the inverse-Compton scenario for the jet’s X-rays, by noting that the maximum plausible jet density is $\rho_{\text{jet}} < 100 m_{\text{H}} \text{ m}^{-3}$. (The latter estimate follows from head velocity estimates for other jets of typically $v_{\text{h}} \approx 10^{-2}c$ (e.g. as collected by Blundell & Rawlings 2000), from asymmetry considerations. The head advance speed is given by $v_{\text{head}} \approx \sqrt{\eta}v_{\text{jet}}$. Since jet velocities v_{jet} are believed to be at least mildly relativistic, and the ambient density in these systems is typically below $10^4 m_{\text{H}} \text{ m}^{-3}$. If these jets were highly relativistic, the jet density would become even lower.)

Here, we present simulations in support of this model (§2). We show how the jet’s density and bulk Lorentz factor can be constrained within our model (§3) and how to test it with future observations (§4).

2. Hydrodynamic model

2.1. Setup

In order to test the hypothesis of a shock lighting up the jet at knot A, we performed axisymmetric hydrodynamic simulations using the code NIRVANA. This is a well-established, second-order accurate 3D MHD code. Its behaviour in jet simulations has been investigated by Krause & Camenzind (2001). Details can be found there and in Ziegler & Yorke (1997).

Since the assumed atmosphere is approximately isothermal, a density decrease is equivalent to a pressure drop and results in an overpressured jet. Heavy, overpressured jets are known to expand radially at the Mach angle (Meier, Sadun, & Lind 1991). Since the jet in 3C 273 is radially resolved and well-collimated (Jester 2001), the Mach number should be high, unless it is magnetically dominated. Trying a pure hydrodynamic model, we adopt an internal Mach number of 94 for the simulation of the jet. We model the surroundings of 3C 273 by a King type atmosphere:

$$\rho(r) = \rho_0 \left[1 + \left(\frac{r}{a} \right)^2 \right]^{-3\beta/2} \quad (1)$$

with $r = \sqrt{R^2 + Z^2}$, $a = 15R_j$, and $\beta = 1.5$.

The simulation is carried out on a grid with 60 jet radii (R_j) in the axial (Z), and 7.5 R_j in the radial (R) direction. The jet is injected steadily in both directions at the center of the grid in a cylindrical box with height $2R_j$ and in initial pressure equilibrium. We use a bipolar simulation to remove the artificial boundary condition on the injection side in many earlier jet simulations, without implying that 3C 273 itself is two-sided. The density contrast (jet/environment) η is initially 0.5 and increases to 70 at $(R, Z) = (0, \pm 30)$.

The gravity of a dark matter halo was adjusted in order to keep the atmosphere in hydrostatic equilibrium. Because of limited computer memory, it is not possible to simulate the entire jet evolution – not even the kpc part which takes place on a scale of several hundred jet radii. Therefore, the atmosphere was not adjusted to observed King profile parameters (see §3 below), but instead designed to retain the important details on a smaller scale: a central plateau region, followed by a steep decrease beyond a turnover point. The jet radius was resolved with 60 points in both directions. At that resolution, global quantities are expected to be accurate on the 5% level (Krause & Camenzind 2001). However, potentially important Kelvin-Helmholtz modes may be unresolved. This is a serious concern. But since full numerical convergence is beyond reach with present computer resources, we consider this as a reasonable compromise.

2.2. Results

Representations of logarithmic density distribution and the jet marker at the final simulation time are shown in Figure 2. The typical constituents of jets are easily recognized: a twin jet beam is injected upward and downward from the center and terminates at a shock. In the central part of the simulation volume, the beam is surrounded by a narrow layer of exhaust jet plasma which extends outward to some peculiar extensions. The jet has displaced and compressed the atmosphere, driving a bow shock around the whole system. We show both sides of the simulated jet in order to emphasise the stability of the discussed features. The simulations show a weak backflow, tightly wrapped around the beam. This is in good agreement with observations (Röser et al. 1996), although the full 3D effects are not covered by our simulation (cf. Tregillis et al. 2001).

The jet and cocoon have their own pressure system and are unaffected by the external pressure. The temporal development is as follows: Due to the high Mach number, the jet builds up a high pressure in the cocoon and the shocked ambient medium of more than ten times the initial jet pressure, and up to several hundred times the pressure in the undisturbed medium. The jet beam contracts due to the high cocoon pressure, causing a strong shock. Both effects together increase the jet density by a factor of 20 at $Z \approx \pm 17$. At that position, the background gas has $\approx 1/3$ of the initial jet density ($\eta = 3$). The shock's position is also marked by the appearance of peculiar filaments. Downstream, the jet expands again, and pressure equilibrium between jet and shocked external gas is soon established in the vicinity of the jet head, the radius being not much different from that at the beginning.

The filaments are approximately 50% denser than their environment. Their pressure is lower than that of the surroundings, and the tracer (Fig. 2) clearly shows that they consist of jet plasma. The filaments form due to a nonlinear Kelvin-Helmholtz instability at the interface between cocoon and shocked ambient medium. Such filaments have never been observed in simulations of light jets, even with similar resolution (Krause & Camenzind 2001). Their appearance is therefore the result of this particular change in density contrast η between jet and surrounding medium from below unity (underdense jet) to above unity (overdense jet). Thus, our simulations show that the proposed change in density contrast is capable of explaining both the lighting up of 3C 273's jet at knot A as result of a collimation shock, and the formation of extensions to the jet close to knot A as filaments of beam plasma disconnected from the main flow.

We repeated the simulation with a lower resolution of 50 points per beam radius. In this case the filaments did not appear. This indicates that the responsible wavelength is $0.018 \pm 0.002R_j$. The position of the jet compression point does not change significantly.

The use of a nonrelativistic approximation even for a relativistic jet is an accepted approach. The decisive point here is the correct representation of growth rates of the Kelvin-Helmholtz instability giving rise to the filamentary extensions. Reynolds, Heinz, & Begelman (2002) point out that the key parameter for this is the ratio of the relativistic enthalpies ($H = \rho c^2 + \gamma_{\text{ad.}} e$, where $\gamma_{\text{ad.}}$ is the adiabatic index and e the internal energy density) in the two neighbouring media. Since the pressure is not comparable to the rest mass anywhere in the presented model, we conclude that the Kelvin-Helmholtz growth rates are calculated correctly in our non-relativistic simulation.

3. Physical parameters of 3C 273 in this model

Many of the detailed physical parameters of jets are unknown, in particular the jet density, jet composition (pair or hydrogen plasma?) and bulk jet Lorentz factor at kiloparsec scales. In our model the density contrast at knot A can be read off from the simulation. Therefore, the jet density can be obtained simply by determining the external density at that location. Furthermore, observations of samples of radio galaxies imply that the kinetic energy Q carried by jets is of the same order as the luminosity Q_{phot} of the accretion disk launching them ($\epsilon = Q/Q_{\text{phot}} = 0.05 \dots 1$; Willott et al. 1999) – Rawlings & Saunders (1991) originally even concluded that Q/Q_{phot} was greater than unity. This allows to write the jet parameters in terms of the disk luminosity as observable, which we take to be the AGN’s bolometric luminosity of $L_{\text{bol}} = 2.5 \times 10^{40}$ W (Ulrich, Maraschi, & Urry 1997). Combining the two, we obtain a relation between the jet Lorentz factor and line-of-sight angle.

3.1. Determination of the jet’s density

X-ray observations of 3C 273’s host galaxy atmosphere provide the external density. Röser et al. (2000) determined the following parameters for a King-profile halo (Eqn. 1) around 3C 273 : $a = 10''8$, $\rho_0 = 6 \times 10^4 m_{\text{H}} \text{m}^{-3}$, $\beta = 0.6758$. However, we have been cautioned that X-ray atmospheres of many clusters harbouring X-ray bright AGN detected by model fitting of ROSAT observations turned out as spurious when observed with *Chandra* (M. Hardcastle 2002, private communication) – for 3C 273, Crawford et al. (1999) obtained very different halo parameters with the same instrument as used by Röser et al. (2000). There are no published determinations of the extended X-ray emission around 3C 273 using *Chandra* or XMM-Newton. Still, values for $\beta \approx 0.6 \dots 0.8$ are typical at least for normal clusters (Vikhlinin, Forman, & Jones 1999), and the core radius near 30 kpc is not counter-intuitive either. Hence we trust the values given by Röser et al. (2000), but we will show

how our results would vary with a differing central density, keeping the core radius and β parameter fixed. We note that the total gas mass deduced for these parameters does lie in the range expected from 3C 273’s host galaxy luminosity ($\approx 10^{11} L_{\odot}$) and typical mass-to-light ratios.

Having established the central density, we deproject the $12''$ distance of knot A from the quasar core with the unknown line-of-sight angle θ to obtain the jet density from Eqn. 1 as

$$\rho_{\text{jet}} = \eta n_0 m_{\text{H}} \left[1 + \left(\frac{12}{10.8 \sin \theta} \right)^2 \right]^{-1.0137}. \quad (2)$$

Taken at face value, the simulation tells us $\eta = 3$ near knot A, but we will use $\eta = 1$ for simplicity and refer to our model as “the $\eta = 1$ model”. Substituting the values discussed above and adopting an inclination of 3° , as suggested by Harris & Krawczynski (2002), we determine a jet density of $100 m_{\text{H}} \text{m}^{-3}$. Since we consider this to be the maximum plausible jet density, we conclude that the $\eta = 1$ model precludes inclinations of more than 3° . However, there is some reason to doubt this line-of-sight angle, as we will point out now.

3.2. The Γ – θ relation

The jet’s kinetic luminosity is

$$L_{\text{kin}} = A \rho_{\text{jet}} B \Gamma (h \Gamma - 1) c^3, \quad (3)$$

where Bc and Γ are the bulk jet velocity and Lorentz factor, respectively. $h = H/\rho_{\text{jet}}c^2$ is the jet’s specific relativistic enthalpy. Since the jet is well-collimated, it can be treated as a cylinder of radius $r_{\text{jet}} = 0''.35$ (Jester 2001). Writing $L_{\text{kin}} = \epsilon L_{\text{bol}}$, we can combine equations 2 and 3 to obtain a relation between the jet bulk Lorentz factor Γ , the line-of-sight angle θ and the external density. We plot this relation in Figure 3. The problem has three parameters: the line-of-sight angle θ , the central density n_0 and the ratio of jet to disc luminosity ϵ . However, the resulting jet bulk Lorentz factor only depends on the ratio n_0/ϵ , which we therefore use as abscissa.

The global trend of $\Gamma(n_0/\epsilon)$ in Figure 3 can be understood as follows: at fixed n_0/ϵ , a smaller line-of-sight angle means the projected $12''$ correspond to a larger deprojected distance, and hence a lower external density at knot A. This means the jet’s bulk Lorentz factor has to increase to achieve the fixed kinetic energy. We have marked on the abscissa the two values corresponding to the central density derived by Röser et al. (2000) with ROSAT for $\epsilon = 0.1$ and $\epsilon = 1$, the range reported by Willott et al. (1999). Assuming this ROSAT

density, it can be seen that the jet Lorentz factor Γ remains in the interval $[1, 2]$ for nearly the entire range of possible values of the line-of-sight angle, from $\theta = 90^\circ$ down to $\theta \approx 3^\circ$ for $\epsilon = 1$, and down to $\theta \approx 1^\circ$ for $\epsilon = 0.1$. Higher Lorentz factors would require an alignment even closer to the line of sight.

Assuming that the jet’s X-ray emission is due to inverse Compton scattering of cosmic microwave background photons, Harris & Krawczynski (2002) derive a much higher Lorentz factor of $\Gamma \approx 20$ and a viewing angle $\theta \approx 3^\circ$. If we assume this angle in our model, we again obtain a much lower jet Lorentz factor of approximately 2 near knot A. Thus, our $\eta = 1$ model is inconsistent with the inverse Compton model and favours the alternative synchrotron model for the jet’s X-ray emission (Röser et al. 2000; Marshall et al. 2001).

In this case, the line-of-sight has no longer to be kept fixed at 3° . We can further change our viewpoint by considering a likely value for the jet density, which is expected to be of the order of $10 m_{\text{H}} \text{m}^{-3}$. The values of Γ corresponding to this jet density for different ϵ have been marked in Figure 3. From the intersection of the corresponding horizontal and vertical dashed lines, it follows from assuming the ROSAT density that $\Gamma \approx 2$ for $\epsilon = 0.1$ and $\Gamma \approx 5$ for $\epsilon = 1$. It also turns out that the ROSAT density corresponds to a line-of-sight angle of $\theta \approx 1^\circ$ for a fixed jet density of $10 m_{\text{H}} \text{m}^{-3}$, independently of the value of ϵ . We consider these values as the most likely region for jet parameters within our model.

3.3. Comparison with other models

The $\eta = 1$ model provides a plausible explanation for the features at knot A. The derived parameters disagree with some other models and observations. However, as we point out in the following, these problems are not insurmountable.

At the base of the kiloparsec-scale jet, VLBI observations imply a line-of-sight angle $\theta \approx 10^\circ$ and a bulk Lorentz factor $\Gamma \approx 10$ for the milliarcsecond jet (Abraham & Romero 1999) – however, there is a change in position angle between this part at 244° and the arcsecond jet considered here at 222° , so it is clear that some change in direction occurs between parsec- and kiloparsec scales.

Both Conway & Davis (1994) and Meisenheimer, Yates, & Röser (1997) independently obtained $\theta \approx 45^\circ$ for the flow near the end of the jet, considering the polarisation change and a physical model of the jet-terminating shock, respectively. This seems to be in conflict with both the $\eta = 1$ model and the inverse Compton model for the X-ray emission. Hence, one has to assume that the flow direction changes between knot A and the hotspot. This is not unexpected since 3D simulations show that jet heads are not stable features but usually

flap around (e.g. Tregillis et al. 2001).

Another way to obtain constraints on the jet’s Lorentz factor from the external density has been shown by Conway et al. (1981): the pressure in the hot spot must exceed the ram pressure of the extragalactic medium at the bow shock, otherwise the hot spot would be disrupted. They obtain a hot spot pressure estimate from the minimum pressure for synchrotron sources. Since the hot spot pressure could not be more than an order of magnitude greater than the minimum pressure without making the jet very inefficient (small ratio of radiated to stored power), we use their estimate here.

Formula 5 given by Conway et al. (1981), together with relativistic momentum flux balance (Scheck et al. 2002; Krause 2002), implies a jet Lorentz factor of at most $\Gamma \approx 2$ when we use the universal density ($n_{\text{universe}} \approx 1 \text{ m}^{-3}$) as a lower limit to the external density at the hot spot. This lower limit, and hence the upper limit $\Gamma \approx 2$, would in fact be achieved for viewing angles below $0^\circ.3$ for the profile parameters given by Röser et al. (2000). However, so small an angle would be inconsistent with our $\eta = 1$ model, which would require a much higher central density for this angle and Lorentz factor (compare Fig. 3). Given the jet’s diameter of $0''.7$ and projected length of nearly $22''$, such small angles would imply that we are looking along nearly 1 Mpc of jet material. The only way to avoid such long line of sights for small viewing angles is a Lorentz factor much higher than we just assumed, in which case relativistic aberration would introduce a difference between the line-of-sight angle and our viewing angle in the jet’s rest frame.

The problem can be solved in two ways: One possibility is that the jet decelerates between knot A and the hotspot. In this case Conway’s argument provides no additional constraint on the inclination. The other possibility is that the density in the halo falls off more steeply than assumed. Röser et al. (2000) determined the density profile out to a radius of 300 kpc. The external density could therefore in principle fall off more steeply than a King profile at large radii. This would not only result in a bulk Lorentz factor of $\Gamma = 2$, but also in a larger inclination for the $\eta = 1$ model.

So far, we implicitly assumed a cold jet (specific enthalpy $h \approx 1$). A larger value of h corresponds to a lower ϵ in our model, and hence results in an even lower value of Γ , and a higher value for θ . From Fig 3 we consider $h > 10$ unlikely, which would increase θ to 3° . If h really was much greater than one, the growth rates for the Kelvin-Helmholtz instability would be different than assumed in our simulation. In this case, the simulation would need to be repeated with a relativistic code, in order to find out if the filaments appear also in a jet with high specific entropy. This is beyond the scope of the present paper.

From Figure 3 it is clear that none of the parameter pairs in the literature simultaneously

fits into our model of $\eta = 1$ at knot A and fulfils the requirement $L_{\text{kin}} = \epsilon L_{\text{bol}}$ with $\epsilon = 0.05 \dots 1$ as determined by Willott et al. (1999). Like the constraints given by Conway et al. (1981), our model favours a low bulk Lorentz factor ($\Gamma \approx 2$ for sensible jet orientations). It is clear that a confirmation of our $\eta = 1$ model, together with better determination of the external density from X-ray data, would be a substantial advance in determining the jet density, and hence the likely values of θ and Γ .

We now summarise our results and discuss which observations are required to test the model we have presented, and thus shed new light on these issues.

4. Summary and future observations

We have presented axisymmetric 2.5D hydrodynamical simulations of a jet propagating in a King atmosphere and crossing from density contrast $\eta = \rho_{\text{jet}}/\rho_{\text{ext}}$ below unity to above unity. A shock forms near the position at which $\eta = 1$ (in fact, closer to $\eta = 3$), and simultaneously the nonlinear Kelvin-Helmholtz instability at the interface between cocoon and shocked ambient medium produces filaments of beam plasma perpendicular to the main flow (Fig. 2). The growth timescales for this instability is essentially the same for a relativistic jet as for the non-relativistic case simulated here (see §2.2).

This instability appearing in our model can explain the morphology of the kiloparsec-scale jet in 3C 273. We identify the jet’s extensions (Fig. 1) with the filaments in the simulation. The onset of bright synchrotron emission at knot A in the jet is due to the pressure increase caused by the shock. This shock could be strong enough to accelerate X-ray synchrotron electrons, and hence may simultaneously account for the nearly unresolved bright X-ray emission associated with this region (Marshall et al. 2001). Our model thus explains both the relatively sudden onset of bright jet emission at all wavelengths near knot A and the appearance of extensions to the jet, whose nature and relation to the jet had been unknown. These statements are not affected by the fact that the jet in 3C 273 is one-sided — we use a bipolar outflow simulation only to avoid arbitrary boundary conditions at the inflow end of the simulation volume.

With an accurate determination of the external medium’s density and the line-of-sight angle, our $\eta = 1$ model achieves a fairly direct determination of the jet density. Employing a line-of-sight angle of 3° , as suggested by the inverse Compton model for the X-ray emission by Harris & Krawczynski (2002), we obtain a jet density of $100 m_{\text{H}} \text{ m}^{-3}$. Alternatively, combining our model with the fact that a jet’s kinetic energy is comparable to the luminosity of the disc launching it (Willott et al. 1999), we obtain a relation between the jet’s bulk

Lorentz factor Γ and the line-of-sight angle θ (Fig. 3). The bulk Lorentz factor predicted by the relation is much lower than required by the inverse Compton model. Setting the jet density to $10 m_{\text{H}} \text{m}^{-3}$ results in a line-of-sight angle of 1° , and Lorentz factors between two and five. The line-of-sight angle can be higher than this if the density profile steepens beyond the radius of 300 kpc, where it has not yet been measured.

This relation between bulk Lorentz factor and line-of-sight angle can also serve as an important constraint for the analysis of other observations which depend on the bulk Lorentz factor, *e.g.*, the explanation of the jet’s X-ray emission as beamed inverse Compton or synchrotron emission. This would greatly benefit from confirming the ROSAT determination of the external density by Röser et al. (2000) with XMM or *Chandra* observations.

Our model does not attempt to explain the detailed run of the surface brightness profiles at radio, optical and X-ray wavelengths. The need for distributed particle acceleration to explain the presence of optical (and possibly X-ray) synchrotron emission along the entire jet beyond knot A, on scales much larger than the synchrotron and inverse Compton loss scales, has been established by Jester et al. (2001). The details of the acceleration mechanism are the subject of ongoing work. Whatever the details, the mechanism needs to dissipate energy stored either in magnetic fields or in the bulk motion of jets (*e.g.*, Litvinenko 1999; Stawarz & Ostrowski 2002; Rieger & Mannheim 2002). It is entirely plausible that the shock occurring at knot A in our model triggers such dissipation mechanisms.

In our model, the jet’s extensions consist of beam plasma. We therefore expect their emission to be synchrotron emission. The spectrum of the southern extension *S* and of *In1*, the inner extension’s eastern knot, are compatible with power laws in the near-infrared through ultraviolet (Jester et al. 2001). However, like for the jet (Röser & Meisenheimer 1991), the proof for synchrotron emission from the extensions would lie in the observation of linear polarisation.

Ground-based polarimetric observations hint at a polarisation of a few percent for the inner extension *In* (Röser & Meisenheimer, unpublished), while the southern extension *S* cannot be separated from the jet at ground-based resolution. The only polarimetric observations with (in principle) sufficient angular resolution are FOC data taken before the Hubble Space Telescope’s spherical aberration was corrected (Thomson, Mackay, & Wright 1993). The published polarisation map indicates a linear polarisation of a few percent for both extensions. However, the detection is only marginally significant. Perlman (2003, private communication) has re-reduced the data and confirms these results only for the southern extension *S*, but obtains zero polarisation for the inner extension *In*. Deep high-resolution polarimetric observations with the Hubble Space Telescope are therefore necessary for a reliable detection of a polarisation signal from the extensions, which would lend strong support

to our model and be a significant advance in our understanding of jet morphology.

Moreover, as our model favours a low Lorentz factor $\Gamma \approx 1\text{--}2$ for the jet's bulk flow, its confirmation would cast strong doubts on the inverse Compton model for the jet's X-ray emission (Harris & Krawczynski 2002), which requires the jet to be highly relativistic ($\Gamma \approx 20$). If correct, our model will therefore favour the alternative explanation of the jet's X-ray emission as synchrotron radiation (Röser et al. 2000; Marshall et al. 2001). Thus, optical polarimetry provides a test for the X-ray emission mechanism as well.

Does this model apply to other jets? The sample of optical jets known today is both small (around 25 as of this writing) and far from being statistically complete. It is therefore unknown what role the external conditions play in lighting up optical jets — all studies of jet sample so far suggest that the detection of an optical jet at present is connected to relativistic beaming and selection effects, not to jet physics (Sparks et al. 1995, 2000; Parma et al. 2003; Jester 2003). 3C 273 is certainly a unique object, being the closest radio-loud quasar. Its jet is equally unique, fulfilling the Fanaroff & Riley (1974) type II criteria but not inflating the usual luminous radio lobe. A similar jet morphology has not been seen elsewhere yet. This may just be the consequence of rare circumstances: an unusually powerful quasar at low redshift, in unusually sparse environs.

Max Camenzind suggested that the jet lights up because $\eta = 1$. Hermann-Josef Röser, Klaus Meisenheimer, Robin Conway and Rick Perley initiated the high-resolution study of 3C 273 with the VLA and the HST. We thank Max Camenzind, Klaus Meisenheimer, and Hermann-Josef Röser for careful readings of the manuscript. This work was supported by the U.S. Department of Energy under contract No. DE-AC02-76CH03000 and by the Deutsche Forschungsgemeinschaft (Sonderforschungsbereich 439).

REFERENCES

- Abraham, Z., & Romero, G. E. 1999, *A&A*, 344, 61
- Blundell, K. M., & Rawlings, S. 2000, *AJ*, 119, 1111
- Clarke, D. A. 1993, in *Lecture Notes in Physics*, Vol. 421, *Jets in Extragalactic Radio Sources*, ed. H.-J. Röser & K. Meisenheimer (Berlin Heidelberg New York: Springer-Verlag), 243
- Conway, R. G., & Davis, R. J. 1994, *A&A*, 284, 724
- Conway, R. G., Davis, R. J., Foley, A. R., & Ray, T. P. 1981, *Nature*, 294, 540

- Crawford, C. S., Lehmann, I., Fabian, A. C., Bremer, M. N., & Hasinger, G. 1999, MNRAS, 308, 1159
- Fanaroff, B. L., & Riley, J. M. 1974, MNRAS, 167, 31P
- Harris, D., & Krawczynski, H. 2002, ApJ, 565, 244
- Jester, S. 2001, PhD thesis, U. Heidelberg, <http://www.ub.uni-heidelberg.de/archiv/1806>
- . 2003, New Astron. Rev., in press [astro-ph/0212397]
- Jester, S., Röser, H.-J., Meisenheimer, K., & Perley, R. 2002, A&A, 385, L27
- Jester, S., Röser, H.-J., Meisenheimer, K., Perley, R., & Conway, R. G. 2001, A&A, 373, 447
- Königl, A., & Choudhuri, A. R. 1985, ApJ, 289, 173
- Krause, M. 2002, PhD thesis, U. Heidelberg, <http://www.ub.uni-heidelberg.de/archiv/2114>
- Krause, M., & Camenzind, M. 2001, A&A, 380, 789
- Litvinenko, Y. E. 1999, A&A, 349, 685
- Liu, F. K., & Zhang, Y. H. 2002, A&A, 381, 757
- Lobanov, A. P., & Zensus, J. A. 2001, Science, 294, 128
- Marshall, H. L., et al. 2001, ApJ, 549, L167
- Meier, D. L., Sadun, A. C., & Lind, K. R. 1991, ApJ, 379, 141
- Meisenheimer, K., Yates, M. G., & Röser, H.-J. 1997, A&A, 325, 57
- Norman, M. L., Winkler, K. H. A., & Smarr, L. 1983, in Astrophysical jets, ed. A. Ferrari & A. G. Pacholczyk (Dordrecht: D. Reidel), 227
- Parma, P., de Ruiter, H. R., Capetti, A., Fanti, R., Morganti, R., Bondi, M., Laing, R. A., & Canvin, J. R. 2003, A&A, 397, 27
- Rawlings, S., & Saunders, R. 1991, Nature, 349, 138
- Reynolds, C. S., Heinz, S., & Begelman, M. C. 2002, MNRAS, 332, 271
- Rieger, F. M., & Mannheim, K. 2002, A&A, 396, 833

- Röser, H.-J., Conway, R. G., & Meisenheimer, K. 1996, *A&A*, 314, 414
- Röser, H.-J., & Meisenheimer, K. 1991, *A&A*, 252, 458
- Röser, H.-J., Meisenheimer, K., Neumann, M., Conway, R. G., & Perley, R. A. 2000, *A&A*, 360, 99
- Scheck, L., Aloy, M. A., Martí, J. M., Gómez, J. L., & Müller, E. 2002, *MNRAS*, 331, 615
- Sparks, W. B., Baum, S. A., Biretta, J., Macchetto, F. D., & Martel, A. R. 2000, *ApJ*, 542, 667
- Sparks, W. B., Golombek, D., Baum, S. A., Biretta, J., de Koff, S., Macchetto, F., McCarthy, P., & Miley, G. K. 1995, *ApJ*, 450, L55
- Stawarz, L., & Ostrowski, M. 2002, *ApJ*, 578, 763
- Stockton, A. 1980, in *IAU Symposia*, Vol. 92, 89
- Thomson, R. C., Mackay, C. D., & Wright, A. E. 1993, *Nature*, 365, 133
- Tregillis, I. L., Jones, T. W., & Ryu, D. 2001, *ApJ*, 557, 475
- Ulrich, M., Maraschi, L., & Urry, C. M. 1997, *ARA&A*, 35, 445
- Vikhlinin, A., Forman, W., & Jones, C. 1999, *ApJ*, 525, 47
- Willott, C. J., Rawlings, S., Blundell, K. M., & Lacy, M. 1999, *MNRAS*, 309, 1017
- Zensus, J. A. 1997, *ARA&A*, 35, 607
- Ziegler, U., & Yorke, H. W. 1997, *Computer Phys. Communications*, 101, 54

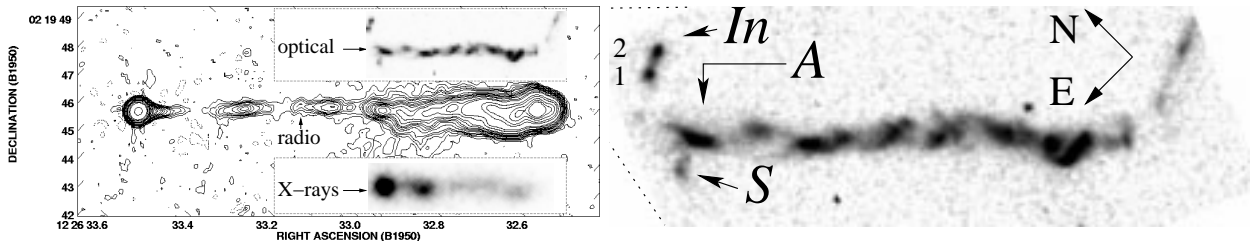


Fig. 1.— Left: The jet in 3C 273 at radio (6 cm VLA image by R. Perley), optical (620 nm HST image from Jester et al. 2001) and X-rays (Chandra image, kindly supplied by H. Marshall; *cf.* Marshall et al. 2001). X-ray and optical image (displaced vertically) are shown for the part of the jet beyond knot A, which is the brightest X-ray feature and marks the onset of bright optical emission. Right: Close-up of the optical jet labeling the features referred to in the paper: the bright region “knot A”, and the “southern extension” *S* and “inner extension” *In*, consisting of two knots *In1* (easternmost) and *In2*. The feature at the far right is most likely a galaxy unrelated to the jet.

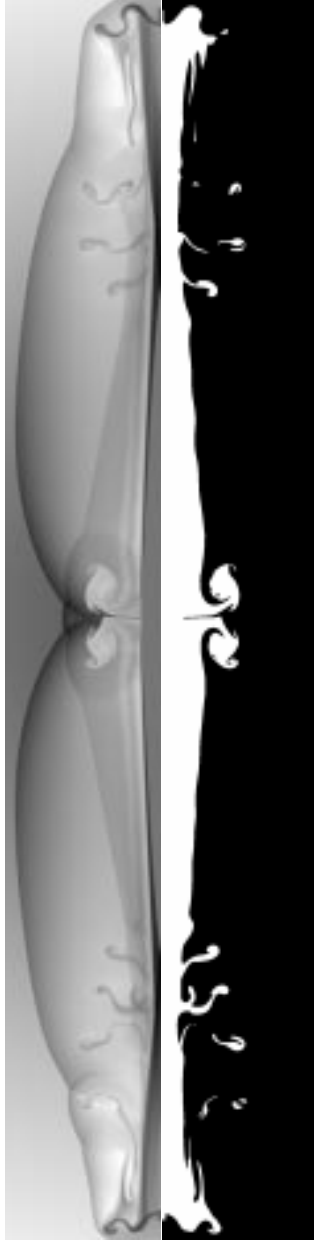


Fig. 2.— Hydrodynamic simulation of a Mach 94 jet which is initially lighter than the surrounding medium by a factor of two. The jet injected in the middle of the grid in both directions. Left: logarithmic density distribution, darker regions represent higher density. Right: marker of beam plasma (white).

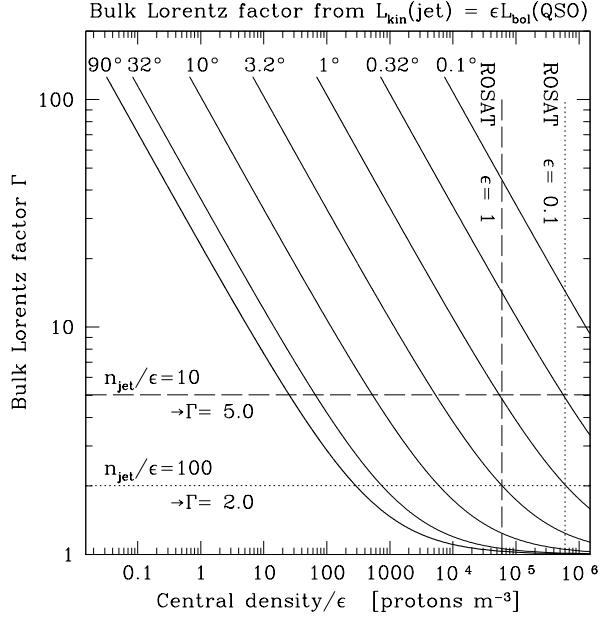


Fig. 3.— 3C 273’s jet bulk Lorentz factor Γ is as function of the galaxy atmosphere’s central density. The relation (solid lines) is shown for various line-of-sight angles, for the maximum 90° (heavy line) and for angles decreasing by factors of $1/\sqrt{10}$ from 32° . It is obtained by setting the jet density equal to the external density at a projected distance of $12''$ (corresponding to the onset of knot A) in a King profile with $\beta = 0.6758$ and core radius $a = 10''8$, and by setting the jet’s kinetic luminosity a fraction ϵ of the quasar’s bolometric luminosity of 2.5×10^{40} W, with $0.1 \lesssim \epsilon \lesssim 1$ (Willott et al. 1999). A value for $n_{\text{jet}} = \rho_{\text{jet}}/m_{\text{H}}$ near 10 m^{-3} might be expected and the corresponding bulk Lorentz factor is shown by the horizontal lines for $\epsilon = 0.1$ (short dash) and $\epsilon = 1$ (long dash), respectively. The value for the central density as quoted by Röser et al. (2000) from ROSAT observations is also marked by vertical lines, again both for $\epsilon = 0.1$ (short dash) and $\epsilon = 1$ (long dash).